# Automatic Identification of EUV structures on the Sun with a Fuzzy Clustering Algorithm


## F. Carella[1] and A. Bemporad[2]

[1] *University of Turin - Physics Department, via Pietro Giuria 1, 10125 Turin, Italy. , e-mail: francesco.carella@edu.unito.it*
[2] *INAF-Turin Astrophysical Observatory, via Osservatorio 20, 10025, Pino Torinese (TO), Italy. , e-mail: alessandro.bemporad@inaf.it*



## Abstract

This technical report describes the first implementation of a Fuzzy c-means (FCM) algorithm for the automatic identification of structures on the Sun based on EUV images and photospheric magnetograms. Before the application of FCM, the AIA 193 Å images and HMI LOS magnetograms acquired by SDO have been pre-processed, and a geometrical approach to correct the limb brightening of EUV images is applied. Then, the images and the magnetograms are analyzed pixel-by-pixel by determining the degree of membership of each pixel to one of clusters, previously defined based on the analysis of a sample training dataset. The routines are written in IDL programming language and will be inserted in the SWELTO pipeline. The work described here was the subject of a Degree Thesis in Physics.



*Keywords:* Space Weather - Coronal Holes - Active Regions - Limb Brightening - Image Processing - Fuzzy Clustering


## 1 Introduction

Space Weather is a branch of heliophysics and space physics dealing with study of the interplanetary magnetic field and phenomena like the solar wind and solar flares, placing a focus on the circum-terrestrial zone: magnetosphere, ionosphere, thermosphere and exosphere. Transient phenomena of solar origin can create electromagnetic disturbances to orbiting devices in the circumterrestrial medium, as well as to electronic devices on Earth. Those disturbances take a variable time to reach the Earth, in a range that goes from a few days to dozens of minutes.

Monitoring the Sun 24h could help us to identify in advance possible regions on the Sun that could cause severe problems and predicting their impact: that's one of the aim of Space Weather. So, an accurate monitoring of coronal holes (CH), quiet sun (QS) and active regions (AR) is extremely important for Space Weather predictions. For this purpose, considering the huge amount of data being routinely acquired by current space- and ground-based observatories, it is becoming more and more important today to develop routines able to automatically identify, track, and monitor solar features.

In this paper we present a series of routines based on the Fuzzy c-means (FCM) algorithm (Bezdek 1981) that allows to automatically identify and separate CH, QS and AR by analyzing EUV 193 Å images and photospheric magnetograms. Clustering techniques are aimed at reducing the amount of data by categorizing or grouping similar features in a data set. Similar techniques have not been widely applied so far to solar data. Thanks to the availability of daily EUV observations provided for the first time by the EIT instrument (Delaboudinière *et al.* 1995) on-board SOHO mission (Domingo, Fleck, and Poland 1995), the possibility to automatically identify and track solar features based on FCM-algo applied to EUV images was tested already a long time ago. A fractal-based fuzzy technique was tested by Revathy, Lekshmi, and Nayar (2005), where the fractal dimension was first computed to create segmented images with a fuzzy-based approach. A similar method was applied also by Barra, Delouille, and Hochedez (2008) (further optimized by Barra *et al.* 2009) to EIT

images acquired with both 171 Å and 195 Å images from 1997 to 2005 allowing the authors to study with Wavelet analysis the rotation rates for AR, QS and CH. More recently, Aranda and Caballero (2010) and Caballero and Aranda (2013) performed a comparative study of clustering methods for detection of AR in EUV images and demonstrate that improved results can be obtained based on region growing image segmentation followed by hierarchical clustering. Significant improvements have been obtained by Verbeeck *et al.* (2013), who combined different algos analyzing not only EUV images, but also visible light images and magnetograms, to identify not only AR, but also sunspots and CH.

In this work we show for the first time that a FCM-algo can be implemented not only based on the ingestion of EUV images, but also in combination with photospheric magnetograms. For this purpose, first we apply a pre-processing to the data acquired by AIA and HMI instruments on-board SDO satellite, to apply a simple geometrical limb brightening correction method for EUV images, and remove noisy regions in MDI images. In the second step, we defined for a sample training dataset different regions of interest corresponding to different clusters, and characterize each of them by measuring the average value of physical quantities such as the EUV intensity and photospheric magnetic field intensity. Then, a FCM algorithm is applied to identify CH, QS and AR and produce segmented images of the Sun. All the routines are written in IDL programming language and have been organized in a pipeline ready to be automatically executed in the SWELTO project of INAF-Turin Astrophysical Observatory.

## 2 Pre-processing of SDO data

The Solar Dynamic Observatory satellite (Pesnell, Thompson, and Chamberlin 2012) supplies routinely EUV images of the solar corona (10-124 nm) thanks to the AIA instrument (Lemen *et al.* 2012), and photospheric magnetograms thanks to the HMI instrument (Scherrer *et al.* 2012). In our work we will focus on the 193 Å -plasma emissions at T $\sim 10^6$ K- filter and LOS (Line of Sight) magnetograms: an example of data analyzed is showed in Figure 1.

The AIA and HMI images are in *fits* format, and are 4096x4096 pixels images, accompanied by a fits header which contains various keywords related to important physical quantities or technical information about instruments and data, such as the projected size of the solar radius, the average intensity (AIA), the average LOS magnetic field intensity (HMI), position of the center of the Sun with respect to the center of the image, etc.

There are substantial differences between the two data: the projected solar disk dimensions aren not the same, in fact each pixel has a different length associated with it on the solar disk and the HMI images are rotated by 180° with respect to AIA images. Hence, it is first necessary to coalign AIA and HMI images.

Hence, for the above image processing we faced two main problems:

- **Coordinates Image Transformation**: in order to optimize the identification of the regions of interest for our algorithm, we have to use the more appropriate coordinates transformation. In this work we choose a spherical transformation, in order to avoid detection of off-limb features, and take into account also projection effects due to the rotation of solar features. Figure 2 shows how the transformation works; the same transformation was applied to EUV images and magnetograms. After coordinate transformation the analyzed images are reduced to (180x180) pixels.
- **Limb Brightening Correction**: Figure 1(a) shows very well a luminosity increase for pixels located toward the solar limb, a physical phenomenon called Limb Brightening. This is a projection effect, due to the fact that in the EUV range the intensity of radiation is proportional to the square of the plasma electron density, and moving out of the solar surface the density decades exponentially as well as the intensity of radiation. Moreover, the coronal plasma is optically-thin: hence we can assume that in each pixel the observed emission comes from a spherical shell with a (almost)

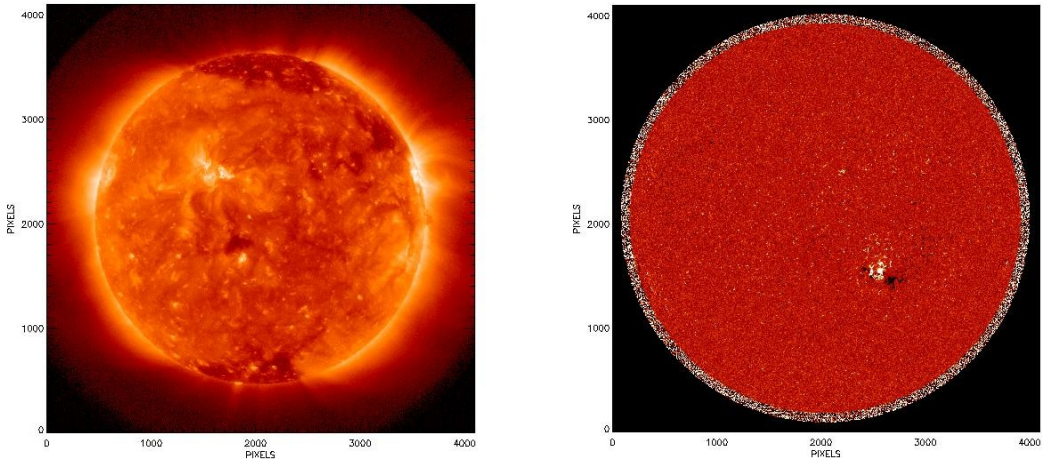


(a) AIA 193 Å image. (06-25-2017 18:00:00)

(b) HMI LOS magnetogram. (06-25-2017 18:00:00)

**Figure 1.** Example of AIA and HMI data.

constant effective thickness. In the end, moving toward the borders of the solar disk, the LOS integration length across the plasma increases, as well as the intensity.

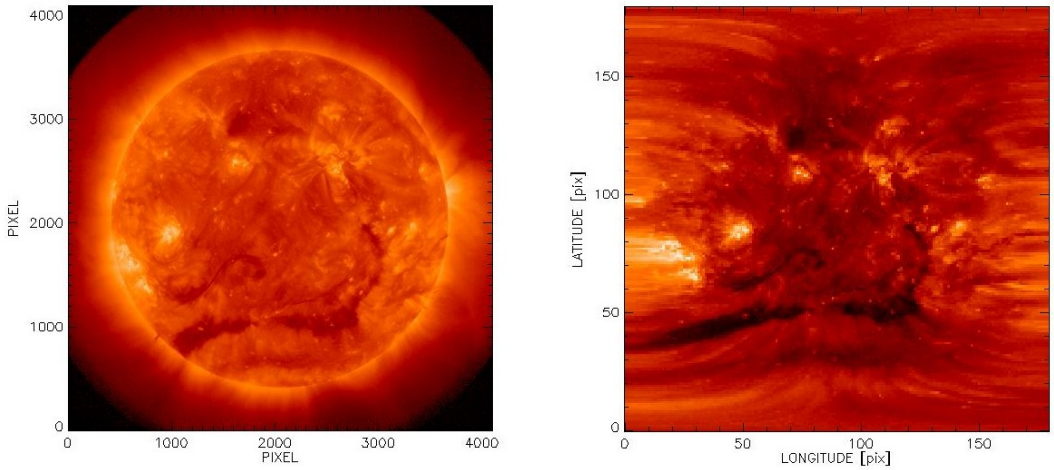


(a) Cartesian coordinates image. (02-18-2013 09:21:30)

(b) Spherical coordinates image. (02-18-2013 09:21:30)

**Figure 2.** Example of spherical transformation on AIA image.

After conversion of HMI images to spherical coordinates, we notice that a further correction is necessary: the HMI aligned and transformed images present a noisy region located near the solar limb at extreme latitudes and longitudes values, where pixels are characterized by values of magnetic field $B$ on the order of $10^8$ Gauss. These few pixels in the spherical transformed image cover a significant amount of pixels. In order to remove this problem, we defined a mask to identify pixels located in this region, and set the magnetic field of each pixel associated with that noisy region equal to 0 (see Figure 3).

## 2.1 Limb Brightening Correction

Before describing the proposed correction, we shall see how the limb brightening affects the intensity variation across the solar disk. In Figure 4 we show how the intensity varies longitudinally along the solar equator after transformation of EUV image in spherical coordinates. The plot shows

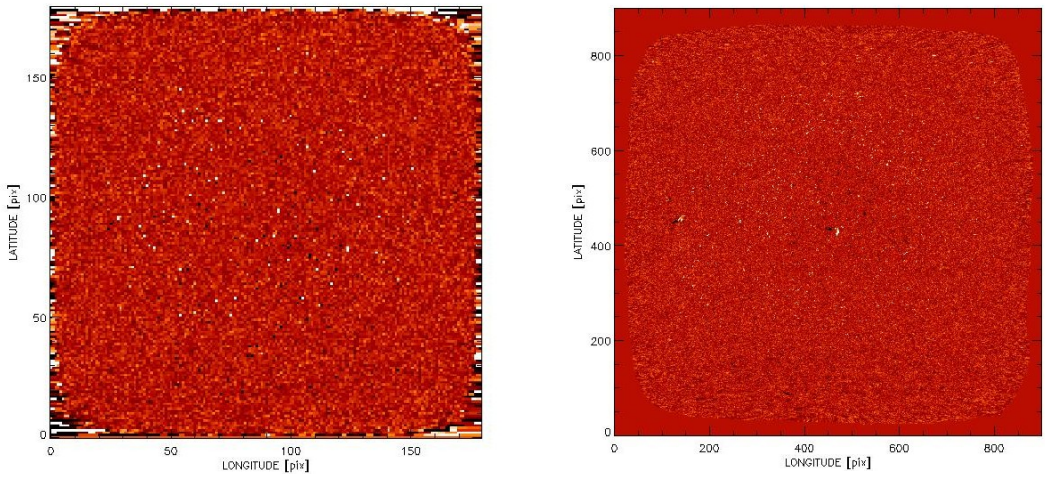


(a) Noisy region on HMI image (black/white pixels). (03-02-2018 18:01:30)

(b) The same image after removal of the noisy regions. (03-02-2018 18:01:30)

**Figure 3.** Correction of noisy region on HMI images.

that the intensity progressively increases going from the center of the solar disk to the solar limb, with two main peaks (corresponding to the location of the solar limb) located at about 500 and 3800 pixels, respectively.

In order to correct the images in spherical coordinates for this effect, we decide to test a simple

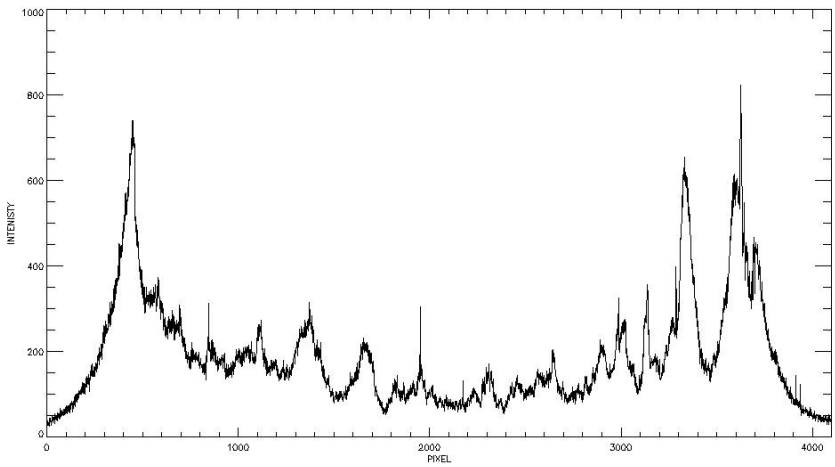


**Figure 4.** Example of limb brightening effect along the solar equator.

geometrical approach described below:

- we consider two spheres concentric on the Sun: the first one has a radius equal to $R = R_{Sun}$, the other one with radius $R' = R_{Sun} + \Delta R$ (as shown in figure 5a);
- for each latitude and longitude $(\theta, \varphi)$, we consider the length $d$ corresponding to the projection of the radial segment $\Delta R$ along the LOS;
- we obtain a geometrical limb function $d(\theta, \varphi)$ that we employ to create a virtual image representing the distribution of limb brightening;
- we divide the image to be analyzed in spherical coordinates by the virtual limb brightening image.

A similar geometrical method was recently described by Cora *et al.* (2019) based on the analysis of data acquired by the UVCS spectrometer (Kohl *et al.* 1995) on-board SOHO. Deviations from a circularly symmetric behaviour (mainly due to the presence of polar coronal holes; see Chargeishvili

*et al.* 2019) were not considered in the first implementation described here. Looking at Figures 5,

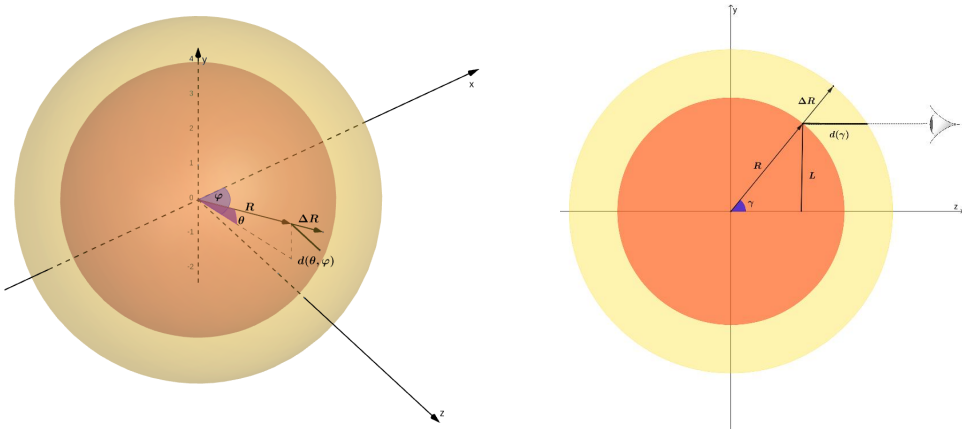


(a) Spherical point of view.

(b) Cilindrical point of view.

**Figure 5.** The representations of the limb function $d(\theta, \varphi)$.

we can see the problem from two points of view: spherical and cylindrical. We parametrize the length $L$ with latitude and longitude $(\theta, \varphi)$ and (because the problem is cylindrically symmetric) introduce an angle $\gamma$ (see Equation 1) in order to derive the relation between these angles (see Equation 2). The length $L$ and the angle $\gamma$ are thus given by:

$$\begin{cases} L = \sqrt{[R_{Sun}\cos(\theta)\cos(\varphi)]^2 + R_{Sun}^2\sin^2(\theta)}, & \theta \in [-\frac{\pi}{2}, \frac{\pi}{2}],\ \varphi \in [0, \pi] \\ L = R_{Sun}\sin(\gamma), & \gamma \in [-\frac{\pi}{2}, \frac{\pi}{2}] \end{cases} \tag{1}$$

$$\gamma = \arcsin\left(\sqrt{\cos^2(\theta)\cos^2(\varphi) + \sin^2(\theta)}\right) \tag{2}$$

Working with cylindrical coordinates we find that:

$$d(\gamma) = \sqrt{R_{Sun}^2\cos^2(\gamma) + \Delta R(2R_{Sun} + \Delta R)} - R_{Sun}\cos(\gamma) \tag{3}$$

But to work in spherical coordinates we have to consider that

$$\cos[\arcsin(x)] = \sqrt{1 - x^2}\,, \quad x \in [-1, 1] \tag{4}$$

and thanks to relation 4 we can express the $d(\gamma)$ function in spherical coordinates, finally obtaining the limb function $d(\theta, \varphi)$:

$$d(\theta, \varphi) = \sqrt{[R_{Sun}\cos(\theta)\sin(\varphi)]^2 + \Delta R(2R_{Sun} + \Delta R)} - R_{Sun}\cos(\theta)\sin(\varphi) \tag{5}$$

The unknown value of $\Delta R$ $[R_{Sun}]$ has been empirically optimized to obtain the best correspondence between the geometric function and the observed limb brightening effect in the considered band-pass filter. From our analysis we conclude that $\Delta R = 0.7 R_{Sun}$ is the best choice for the optimization, as shown in Figure 6. With the obtained symmetric limb brightening function, we create a virtual image whose pixels correspond to the values of the function at the corresponding latitude and longitude. An example in Cartesian coordinates is shown in Figure 7. Then, we divide the EUV normalized image with the virtual limb brightening image, obtaining the results shown in Figure 8.

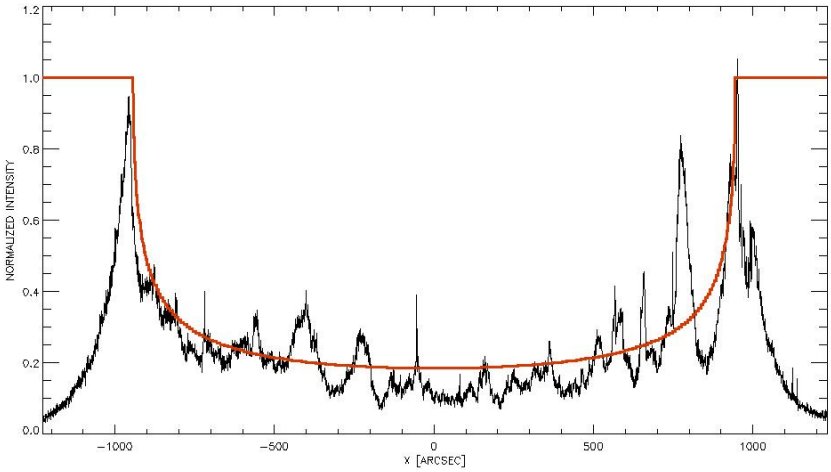


**Figure 6.** The geometric limb brightening function (red curve) in comparison with the observed intensity trend along the solar equator (each curve has been previously normalized).

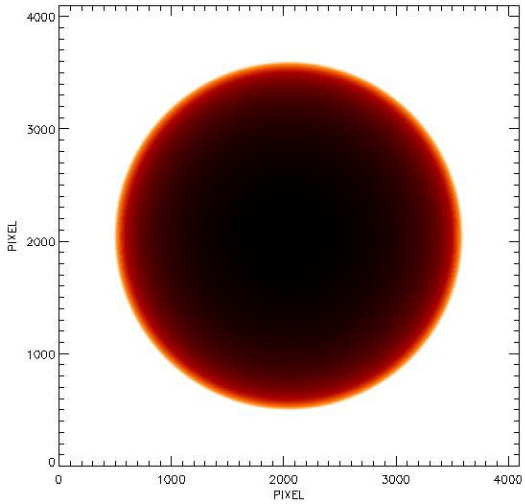


**Figure 7.** Virtual EUV limb brightening image in Cartesian coordinate.

## 3 Definition of Regions of Interest (ROIs)

After the above images processing, we study the intensity in EUV (from AIA data) and the intensity of the magnetic field (from HMI data) by defining region of interest (ROIs) representative of coronal holes (CH), active regions (AR) and quiet sun (QS). This step is of fundamental importance to derive the starting values (centroids) of iteration for the FCM algorithm (see below). These are the steps we followed for our study based on ROIs:

- we choose a EUV images training data sample to work with full resolution images showing well defined CH and AR features;
- we manually proceed with the identification of the ROIs in the EUV images (by employing the IDL routine DEFROI);
- we create arrays containing the coordinates of each pixel belonging to the ROIs previously identified;
- we employ the same ROIs defined from EUV images also for the HMI magnetograms.

Once the ROIs are defined for each image in the training dataset, for each ROI we take the average value and the standard deviation of intensity in the EUV and the absolute value of the intensity of

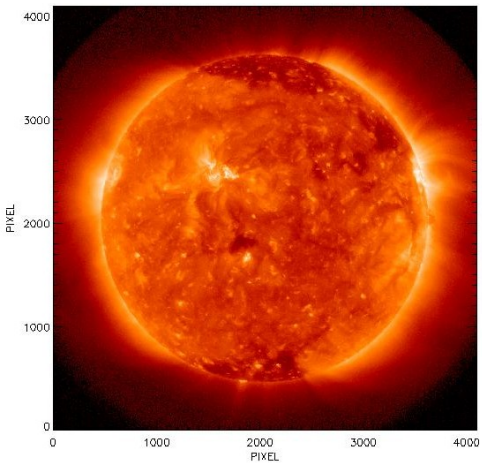


(a) AIA 193 Å image **before** limb brightening removal. (06-25-2017 18:00:00)

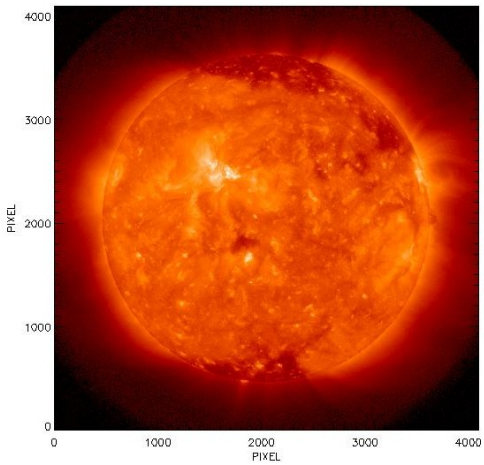


(b) AIA 193 Å image **after** limb brightening removal. (06-25-2017 18:00:00)

**Figure 8.** The result of the limb brightening correction.

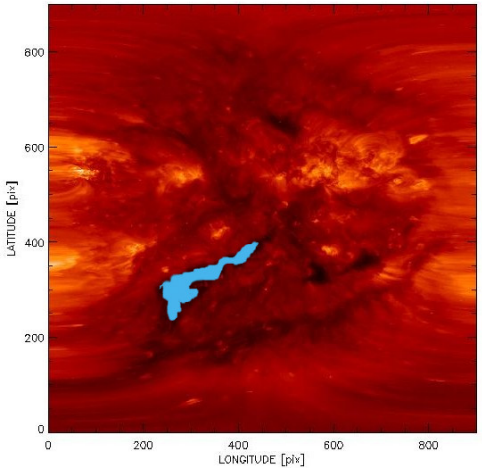


(a) Example of AIA 193 Å ROI (blue region) identifying a mid-latitude CH. (02-03-2012 18:00:00)

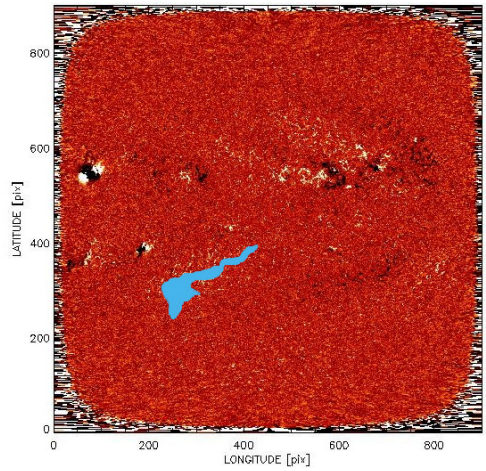


(b) The same ROI superposed onto HMI magnetogram. (02-03-2012 18:00:00)

**Figure 9.** Example of ROI definition.

magnetic field. We do this for about ten images acquired over different years and different solar activity periods, obtaining about 20 average values and standard deviations for each ROI.
During the analysis we defined with ROIs four different kind regions: polar coronal hole (PCH), mid-latitude coronal hole (MCH), active regions (AR) and quiet sun (QS). During the analysis we notice that concerning variations of EUV intensity and photospheric magnetic field intensity, mid-latitude coronal holes seems to have higher values than polar ones. In order to characterize each region, we take the average value among all averages over all pixels belonging to the same kind of ROIs, obtaining the results shown in Table 1. Once starting values for different regions (that will correspond to centroids of different clusters) have been measured, we can proceed with the definition of the clustering algorithm.

| ROI | I [units] | \|B\| [G] |
|---|---|---|
| PCH | 0.144 | 9.002 |
| MCH | 0.309 | 9.957 |
| AR | 6.955 | 94.573 |
| QS | 1.025 | 8.156 |

**Table 1.** Average values from different regions of interest.

# 4 Fuzzy Clustering

## 4.1 Generalities

To automatically identify coronal regions we use a Fuzzy c-means (FCM) algorithm (as defined by Bezdek 1981): each pixel is associated with a probability to belong to one class (or cluster) rather than another (once the clusters have been defined). Doing so, we can subdivide a data set X into $k$ subsets (clusters) which are pairwise disjoint, non-empty and overall reproduce X.
Let us consider a set of N objects $X = x_1, x_2, ..., x_N$, where each $x_i$ is a d-dimensional vector ($x_i \in R^d$). In our case, these N objects are the number of pixels of images (180x180).

**Definition 1** (Fuzzy Clustering)**.** *We define as **fuzzy clustering** a collection of k clusters $C_1, C_2, ..., C_k$ and a **partition matrix** (Fuzzy Partition) $U = u_{ij}$ with $u_{ij} \in [0, 1]$, $i = 1, ..., N$ e $j = 1, ..., k$ ($U \in \mathbb{R}^{k \times N}$) where for each $u_{ij}$ we associate a **membership function** which represents the **membership degree** of the object $i$ to the cluster $C_j$.*

The partition matrix has to satisfy the following properties:

$$\sum_{j=1}^{k} u_{ij} = 1 \qquad\qquad 0 < \sum_{i=1}^{N} u_{ij} < N \tag{6}$$

For each cluster, we associate a **centroid** $c_j$ which defines the characteristics of certain cluster: $c_j \in \mathbb{R}^d$ (in our case, the centroids will be initialized with the values previously obtained from the study of ROIs in Table 1).

**Definition 2** (FCM Functional)**.** *Let be $J_m$: $M_{fc}\, x\, \mathbb{R}^{k \times N} \rightarrow \mathbb{R}$:*

$$J_m(U, \mathbf{c}) = \sum_{i=1}^{N} \sum_{j=1}^{k} (u_{ij})^m (d_{ij})^2 \tag{7}$$

*where:*

- $U \in M_{fc}$ *is the fuzzy partition matrix;*
- $\mathbf{c} = (\mathbf{c}_1, \mathbf{c}_2, ..., \mathbf{c_k}) \in \mathbb{R}^{kd}$ *con* $\mathbf{c_j} \in \mathbb{R}^d$ *is the set of clusters' centroids;*
- $(d_{ij})^2 = ||x_i - c_j||^2$ *dove* $||\cdot||$ *is a **norm** induced by any inner product* $\mathbb{R}^N$*;*
- $m \in [1, \infty)$ *is a **weight exponent**.*

An optimal fuzzy clusterings of X are defined as pairs of $(\widetilde{U}, \widetilde{c})$ that locally minimize the fuzzy C-mean functional $J_m$ (Definition 2). For $m > 1$, $(\widetilde{U}, \widetilde{c})$ may be locally optimal only if:

$$\widetilde{u}_{i,j} = \frac{1}{\sum_{z=1}^{k} \left[ \frac{d_{ij}}{d_{iz}} \right]^{\frac{2}{m-1}}} \tag{8}$$

$$\widetilde{\mathbf{c}_\mathbf{j}} = \frac{\sum_{i=1}^{N} (u_{ij})^m \mathbf{x_i}}{\sum_{i=1}^{N} (u_{ij})^m} \tag{9}$$

Now, we have all the ingredients to show how the FCM algorithm works. From a computational point of view (by using the Bezdek algorithm) the steps are:

1. Choose the number of features $d$ to characterize each data, the number of clusters $c$, and the metrics;
2. Initialize the fuzzy partition matrix $U^{(0)}$ (where 0 indicates that we are at the first iteration);
3. Calculate the values of centroids to be assigned with the formula 9, using $U^{(s)}$, where $s$ indicates the number of iterations;
4. Update the matrix $U^{(s)}$ with the formula 8 with the $\widetilde{\mathbf{c}_\mathbf{j}}$ just calculated;
5. Given a **threshold value** $\epsilon$ and a matricial norm, if $||U^{(s+1)} - U^{(s)}|| > \epsilon$ then we repeat steps 3 and 4, otherwise the algorithm stops.

### 4.2 Application to solar structures

Now, we can proceed to apply the FCM algo to identify solar structures. First of all, we consider four clusters: polar coronal hole (PCH), mid-latitude coronal hole (MCH), quiet sun (QS) and active region. A distinction between PCH and MCH is very important for Space Weather applications. In fact, MCH are usually a source of high speed solar wind streams (HSS) propagating nearby the ecliptic plane, and thus potentially directed towards the Earth as these streams are dragged by solar rotation.

We characterize each points of our algorithm considering three features: EUV 193 Å intensity normalized to the maximum value (to apply the algorithm on any period of the solar activity cycle), absolute value of the photospheric magnetic field (normalized with the absolute value of the average magnetic field of the image we are analyzing), and normalized latitude (with values varying between -1 and 1) to separate among PCH and MCH.

Each point of our algorithm is a vector of this type: $\mathbf{x}_i = (I_i, |B_i|, L_i)$ with $i = 1, ..., N$ (N=number of pixels). The same for centroids $c_j$ with $j = 1, ..., 4$ (1:PCH, 2:MCH, 3:AR, 4:QS).

Setting $m = 1, \epsilon = 0.01$ and the $U^{(0)}$ matrix with values between 0 and 1, the FCM algorithm can start. Once the algorithm stops, we obtain $U^{(s)}$ (where, generally $s < 25$): this matrix represent the probability of each pixel to belong to a certain cluster (an example of probability distribution is shown in Figure 10). Thanks to the $U^{(s)}$ we can create a segmentation of the input solar image.

## 5 Results

For the first test we analyzed AIA and HMI data acquired around the minimum of solar activity cycle, where the sun is "quiet". The results are shown in Figure 11: the FCM converges, polar coronal holes are identified as well as active regions, but the algorithm seems to have some difficulties to distinguish between mid-latidude coronal holes and quiet sun. This is probably due to the defined latitude feature, which apparently seems to apply more restrictions than we expected, probably due to the fact that, from data, the characterization values of this regions are too similar for FCM.

For the second test we selected a time period near the minimum of solar activity when a big mid-latitude coronal hole was also present. The results from the algo are shown in Figure 12. In this case the polar coronal holes have been identified, as well as active regions, but the most important result is that the mid-latitude coronal hole has been identified as well; this is a good result. Also in this case at certain latitude the FCM encountered some difficulties to distinguish MCH from QS, the probable reason has been said previously.

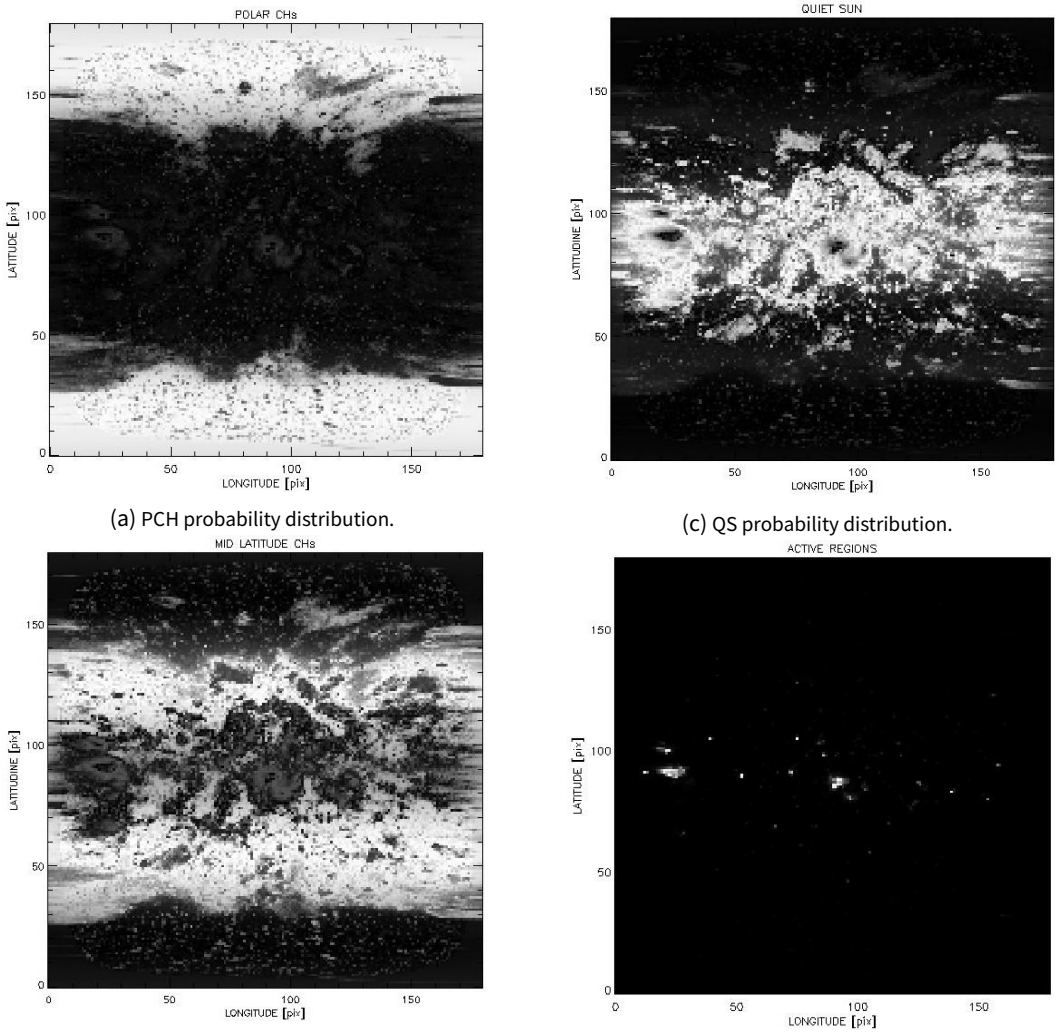


(a) PCH probability distribution.

(c) QS probability distribution.

(b) MCH probability distribution.

(d) AR probability distribution.

**Figure 10.** Example of probability distribution obtained by the matrix $U^{(s)}$: the images are in grey scale, black pixels are associated to probability 0 and white ones to 1.

## 6 Conclusions and future developments

In this paper we describe a pipeline consisting of various routines (written in IDL), for:

1. spherical transformation of solar images;
2. co-alignement of AIA and HMI images;
3. geometrical correction of EUV limb brightening;
4. extraction of mean values by using different ROIs;
5. use of fuzzy clustering algorithm to automatically identify coronal structures;
6. creation of segmented images of the Sun.

The FCM algorithm developed here needs more test. In fact, although it gives acceptable results for images acquired at the minimum of solar activity cycle, for the maximum of solar cycle the results are not yet acceptable, as shown in Figure 13.

This pipeline is part of the SWELTO - Space WEather Laboratory in Turin Observatory - a project aimed at developing new tools for automatic data analysis and future applications of Space Weather forecasting. After a first test at the Turin Observatory, these tools can be further developed and put into execution at the nascent ASI SPace weather InfraStructure (ASPIS) (Plainaki *et al.* 2018) coordinated by the Italian Space Agency (ASI).

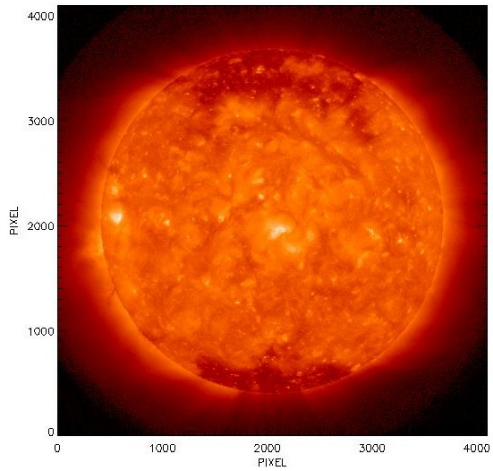


(a) AIA 193 Å minimum image in Cartesian coordinates. (02-03-2018 18:00:04)

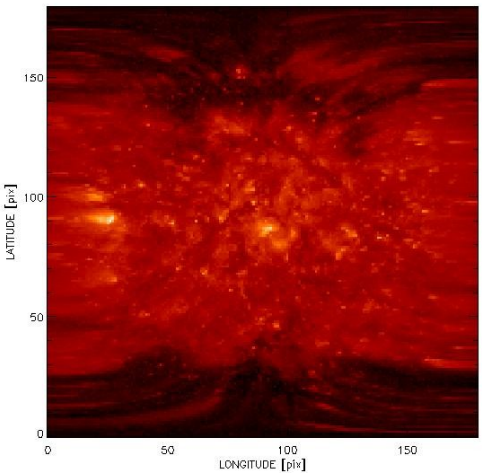


(c) AIA 193 Å minimum image in spherical coordinates.

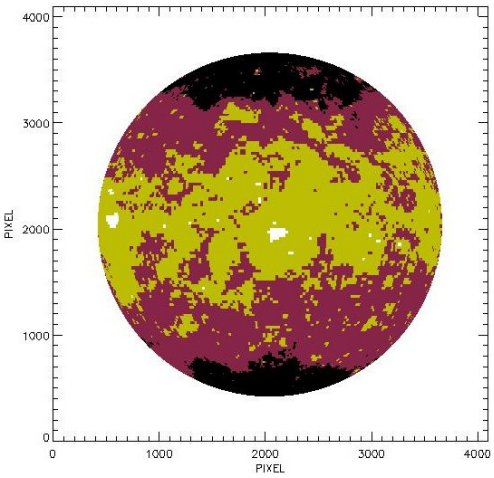


(b) FCM segmentation in Cartesian coordinates.

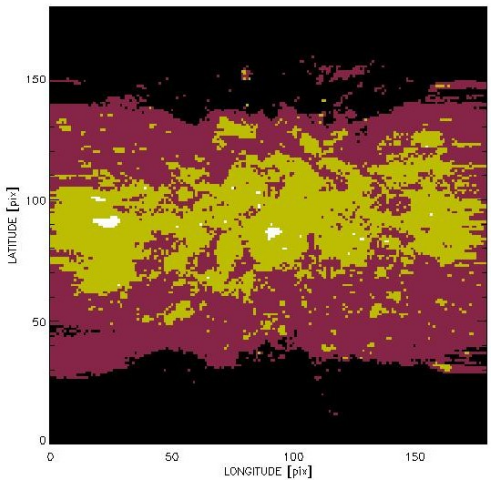


(d) FCM segmentation in spherical coordinates.

**Figure 11.** The results of the first test of the FCM clustering on a minimum image: in black PCH, in purple MCH, in green QS and in white AR.

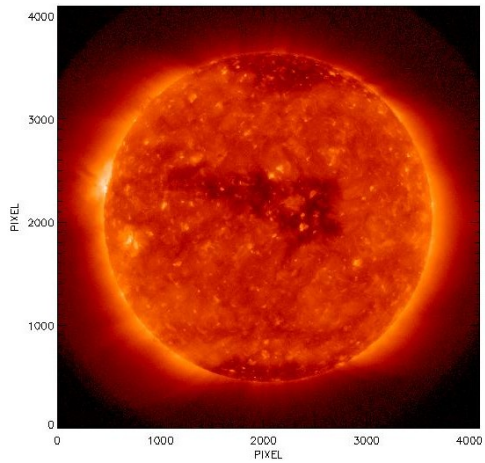


(a) AIA 193 Å minimum image in Cartesian coordinates. (05-04-2018 18:00:00)

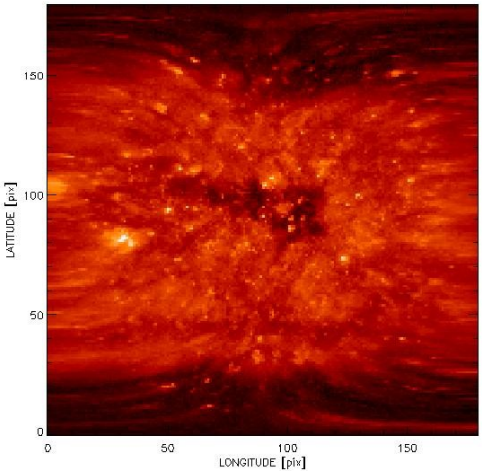


(c) AIA 193 Å minimum image in spherical coordinates.

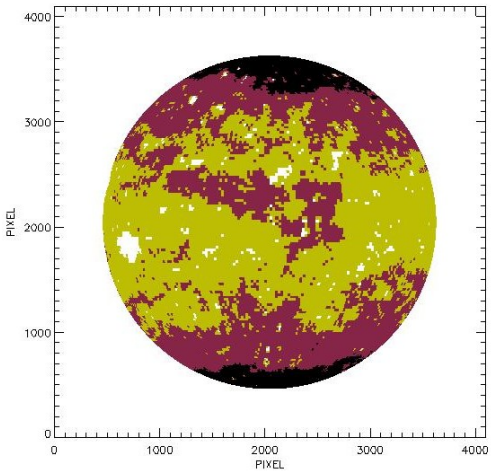


(b) FCM segmentation in Cartesian coordinates.

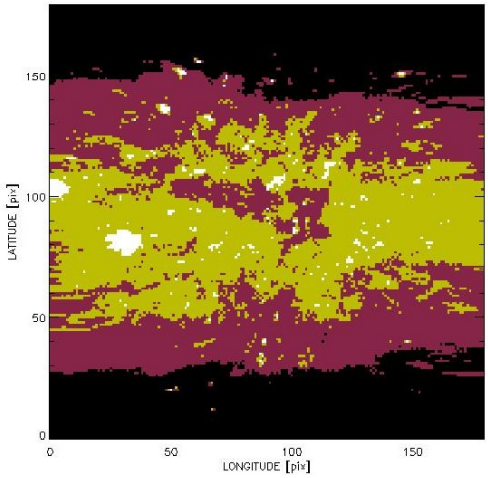


(d) FCM segmentation in spherical coordinates.

**Figure 12.** The results of FCM clustering tested on a mid latitude coronal hole. The colors of the segmentation are the same as Figure 11.

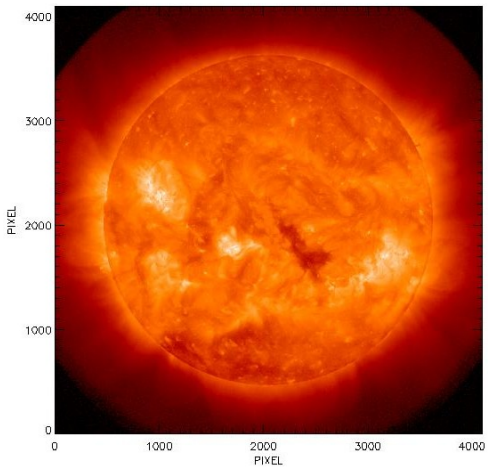


(a) AIA 193 Å maximum Cartesian image. (06-25-2014 18:00:00)

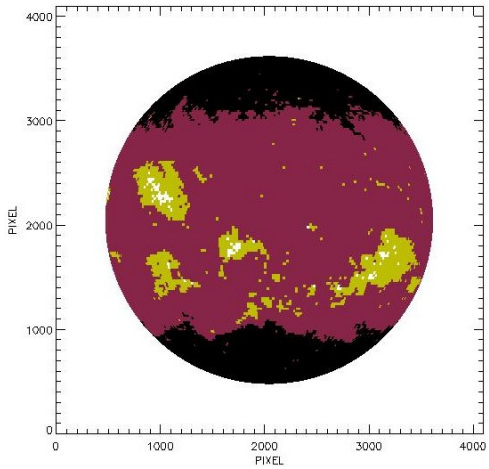


(b) Cartesian segmentation.

**Figure 13.** Results of FCM for a maximum image: there's a constraint induced (probably) by the latitude parameter.

## References


Aranda, M. C., and C. Caballero. 2010. “Automatic Detection of Active Region on EUV Solar Images Using Fuzzy Clustering,” 6178:69–78. June. doi:10.1007/978-3-642-14049-5_8.

Barra, V., V. Delouille, M. Kretzschmar, and J. .-.-F. Hochedez. 2009. “Fast and robust segmentation of solar EUV images: algorithm and results for solar cycle 23.” 505, no. 1 (October): 361–371. doi:10.1051/0004-6361/200811416.

Barra, V., V. Delouille, and J.-F. Hochedez. 2008. “Segmentation of extreme ultraviolet solar images via multi-channel fuzzy clustering.” *Advances in Space Research* 42, no. 5 (September): 917–925. doi:10.1016/j.asr.2007.10.021.

Bezdek, J. C. 1981. *Pattern Recognition with Fuzzy Objective Function Algorithms.* Norwell, MA, USA: Kluwer Academic Publishers. ISBN: 0306406713.

Caballero, C., and M. C. Aranda. 2013. “A Comparative Study of Clustering Methods for Active Region Detection in Solar EUV Images.” 283, no. 2 (April): 691–717. doi:10.1007/s11207-013-0239-2.

Chargeishvili, B. B., D. A. Maghradze, D. R. Japaridze, N. B. Oghrapishvili, T. G. Mdzinarishvili, K. B. Chargeishvili, and B. M. Shergelashvili. 2019. “Variation of coronal holes latitudinal distribution: Correction of limb brightening of EUV coronal images.” *Advances in Space Research* 64, no. 2 (July): 491–503. doi:10.1016/j.asr.2019.04.009.

Cora, A., D. Marocchi, S. Giordano, and L. Zangrilli. 2019. “Solar limb brightening observed with SOHO/UVCS.” *Nuovo Cimento C Geophysics Space Physics C* 42, no. 1, 28 (January): 28. doi:10.1393/ncc/i2019-19028-7.

Delaboudinière, J. .-.-P., G. E. Artzner, J. Brunaud, A. H. Gabriel, J. F. Hochedez, F. Millier, X. Y. Song, *et al.* 1995. “EIT: Extreme-Ultraviolet Imaging Telescope for the SOHO Mission.” 162, nos. 1-2 (December): 291–312. doi:10.1007/BF00733432.

Domingo, V., B. Fleck, and A. I. Poland. 1995. “The SOHO Mission: an Overview.” 162, nos. 1-2 (December): 1–37. doi:10.1007/BF00733425.

Kohl, J. L., R. Esser, L. D. Gardner, S. Habbal, P. S. Daigneau, E. F. Dennis, G. U. Nystrom, *et al.* 1995. “The Ultraviolet Coronagraph Spectrometer for the Solar and Heliospheric Observatory.” 162, nos. 1-2 (December): 313–356. doi:10.1007/BF00733433.

Lemen, J. R., A. M. Title, D. J. Akin, P. F. Boerner, C. Chou, J. F. Drake, D. W. Duncan, *et al.* 2012. “The Atmospheric Imaging Assembly (AIA) on the Solar Dynamics Observatory (SDO).” 275, nos. 1-2 (January): 17–40. doi:10.1007/s11207-011-9776-8.

Pesnell, W. D., B. J. Thompson, and P. C. Chamberlin. 2012. “The Solar Dynamics Observatory (SDO).” 275, nos. 1-2 (January): 3–15. doi:10.1007/s11207-011-9841-3.

Plainaki, C., B. Negri, M. Castronuovo, and A. Antonelli. 2018. “Towards an Italian Space Weather Infrastructure: the ASPIS project.” In *EGU General Assembly Conference Abstracts,* 5239. EGU General Assembly Conference Abstracts. April.

Revathy, K., S. Lekshmi, and S. R. P. Nayar. 2005. “Fractal-Based Fuzzy Technique For Detection Of Active Regions From Solar Images.” 228, nos. 1-2 (May): 43–53. doi:10.1007/s11207-005-6880-7.

Scherrer, P. H., J. Schou, R. I. Bush, A. G. Kosovichev, R. S. Bogart, J. T. Hoeksema, Y. Liu, *et al.* 2012. “The Helioseismic and Magnetic Imager (HMI) Investigation for the Solar Dynamics Observatory (SDO).” 275, nos. 1-2 (January): 207–227. doi:10.1007/s11207-011-9834-2.

Verbeeck, C., P. A. Higgins, T. Colak, F. T. Watson, V. Delouille, B. Mampaey, and R. Qahwaji. 2013. “A Multi-wavelength Analysis of Active Regions and Sunspots by Comparison of Automatic Detection Algorithms.” 283, no. 1 (March): 67–95. doi:10.1007/s11207-011-9859-6.